

# Torsional effect on track support structures of railway turnouts crossing impact

Sae Siew, James ; Mirza, Olivia ; Kaewunruen, Sakdirat

DOI:

[10.1061/JTEPBS.0000004](https://doi.org/10.1061/JTEPBS.0000004)

License:

None: All rights reserved

*Document Version*

Peer reviewed version

*Citation for published version (Harvard):*

Sae Siew, J, Mirza, O & Kaewunruen, S 2017, 'Torsional effect on track support structures of railway turnouts crossing impact', *Journal of Transportation Engineering, Part A: Systems*, vol. 143, no. 2.  
<https://doi.org/10.1061/JTEPBS.0000004>

[Link to publication on Research at Birmingham portal](#)

**Publisher Rights Statement:**

(c) ASCE. Final version of record published as above.

First Validated Feb 2016

**General rights**

Unless a licence is specified above, all rights (including copyright and moral rights) in this document are retained by the authors and/or the copyright holders. The express permission of the copyright holder must be obtained for any use of this material other than for purposes permitted by law.

- Users may freely distribute the URL that is used to identify this publication.
- Users may download and/or print one copy of the publication from the University of Birmingham research portal for the purpose of private study or non-commercial research.
- User may use extracts from the document in line with the concept of 'fair dealing' under the Copyright, Designs and Patents Act 1988 (?)
- Users may not further distribute the material nor use it for the purposes of commercial gain.

Where a licence is displayed above, please note the terms and conditions of the licence govern your use of this document.

When citing, please reference the published version.

**Take down policy**

While the University of Birmingham exercises care and attention in making items available there are rare occasions when an item has been uploaded in error or has been deemed to be commercially or otherwise sensitive.

If you believe that this is the case for this document, please contact [UBIRA@lists.bham.ac.uk](mailto:UBIRA@lists.bham.ac.uk) providing details and we will remove access to the work immediately and investigate.

1 REVISION OF TECHNICAL PAPER

2  
3 “Torsional effect on track support structures of railway turnouts crossing impact”

4  
5 (Title contains 11 words)

6  
7  
8 by

9  
10 **James Sae Siew**

11 School of Civil Engineering  
12 University of Western Sydney, Penrith, NSW, Australia

13  
14 **Olivia Mirza**

15 School of Civil Engineering  
16 University of Western Sydney, Penrith, NSW, Australia

17  
18 and

19  
20 **Sakdirat Kaewunruen**

21 Birmingham Centre for Railway Research and Education,  
22 University of Birmingham, Birmingham, UK

23  
24  
25  
26  
27 Submitted to  
28 ASCE Journal of Transportation Engineering

29  
30  
31  
32 Corresponding Author:

33  
34 Sakdirat Kaewunruen  
35 Senior Lecturer in Railway and Civil Engineering  
36 School of Engineering, University of Birmingham, Birmingham, UK  
37 e-mail: s.kaewunruen@bham.ac.uk

38  
39  
40  
41 Manuscript Summary:

42 Total pages 29 (including 1-page cover)  
43 Number of figures 13  
44 Number of tables 2

# Torsional effect on track support structures of railway turnouts crossing impact

James Sae Siew<sup>1</sup>, Olivia Mirza<sup>2</sup>, and Sakdirat Kaewunruen<sup>3</sup>

**Abstract:** The introduction of special crossings and rail turnouts provides flexibility in the rail network as it allows for vehicles to switch between various tracks, therefore maximizing the utilisation of current infrastructure. Turnouts are a costly and critical feature to a rail system as they suffer adverse operational loads, in comparison to a straight rail track, and thus require regular maintenance. This leads to the question of whether a turnout can be justified for flexibility in comparison to upkeep costs throughout the life of the turnout. Therefore, great consideration is given to the interaction between the turnout components, and reducing wear in service, as failed components may have adverse effects on the performance of neighbouring components. This paper herein presents a development of 3D finite element (FE) model, fostering nonlinearities in materials' behaviours, in order to analyse the forces and reactions within a railway turnout system. The analysis provide new findings of critical sections within the turnout and further enables alterations to be made to initial design of members in order to accommodate for the increased effects. The FE model comprises of standard concrete sleepers with 60 kg/m rail, and with a tangential turnout radius of 250 m. The turnout structure is supported by a ballast layer, which is represented by a deformable solid. The FE model is the world first to predict the torsional behaviour of the turnout and its fragile support by considering multi-wheel impacts which would simulate in-service and cyclic loading, and will be adapted as a set of concentrated loads to represent a coupled locomotive negotiating the turnout. The simulations demonstrate the significance of the third medium to suppress the torsional effect of the crossing forces on supporting bearers.

**Keywords:** Torsional effect; Turnouts; Railroad; Dynamic analysis; Ballasted railway track; Bearers, Sleepers; Crossties.

---

<sup>1</sup> Formerly Honours Student in Civil Engineering Program, School of Civil Engineering, University of Western Sydney, Penrith, NSW 2057 Australia

<sup>2</sup> Senior Lecturer in Civil Engineering, School of Civil Engineering, Western Sydney University, Penrith, NSW 2057 Australia; e-mail: o.mirza@westernsydney.edu.au

<sup>3</sup> Corresponding author; Birmingham Centre for Railway Research and Education, School of Engineering, University of Birmingham, Birmingham, UK. e-mail: s.kaewunruen@bham.ac.uk; sakdirat@hotmail.com, Formerly, Technical Specialist, RailCorp, Sydney NSW 2000 Australia; and a visiting executive fellow at Department of Civil and

## 79 **Introduction**

80           One of the great accomplishments during the early 19<sup>th</sup> century was the development of  
81 railways. The realisation of railways spurred exponential industrial growth for it enabled this mode  
82 of land transportation, which focuses on mass-freightage, to be reliable and economical. The  
83 effectiveness of rail is based upon the general concept of providing a track that is both minimal in  
84 space and material, and yet be able to provide a low-friction, guided medium. The introduction of  
85 special crossings and turnouts provided flexibility in the rail network as it allowed for vehicles to  
86 switch between various tracks, and in-turn reducing the amount of tracks needed.

87           A turnout is a critical part of the railway where a track crosses over one another at an angle  
88 to divert a train from the original track. The railway track and turnouts consists of rails, switches,  
89 crossings, sleeper plates, sleepers, ballast and subgrade (as shown in Figure 1). As above  
90 mentioned, turnouts are an essential part of a rail system as they provide great flexibility, but at the  
91 same time, turnouts are a costly feature to a rail system as they suffer adverse operational loads, in  
92 comparison to an open plain rail track, and require regular maintenance. This leads to the question  
93 of whether a turnout can be justified for flexibility in comparison to the cost of maintenance  
94 throughout the life of the turnout. Turnout components can be designed with stronger, hard wearing  
95 materials as an option to help reduce maintenance costs. When designing, and maintaining, the  
96 railway systems, great consideration is given to the interaction between the turnout components in  
97 service. Due to the particular geometry of wheel–rail contact and sudden variation of track  
98 flexibility, severe impact loads may occur during train passage over the turnout. Turnout  
99 components are subjected to general wear, rolling contact fatigue and accumulated irreversible  
100 (plastic) deformations (Kassa and Nielsen, 2008a; Kaewunruen, 2010, 2013a; 2013b).

101           During their life cycles, railway track structures experience static, dynamic and often impact  
102 loading conditions due to wheel/rail interactions associated with the abnormalities in either a wheel  
103 or a rail. Especially at turnouts crossing, the wheel rail interaction at the transfer zone often causes

104 detrimental impact forces and excessive dynamic actions (Remennikov and Kaewunruen, 2008;  
105 Kaewunruen and Remennikov, 2008; 2009a; 2009b; 2010). Recent studies showed that it is very  
106 likely that a railroad turnout bearers or crossties could be subjected to severe impact loads, resulting  
107 in a rapid deterioration of its structural integrity and durability (Esveld, 2001; Kaewunruen, 2007;  
108 Kaewunruen et al., 2014). Traditional turnout generally imparts high impact forces on to structural  
109 members because of its blunt geometry and the gaps between mechanical connections between  
110 closure rails and switch rails (i.e. heel-block joints). Although a new method of geometrical design  
111 has been adopted for tangential turnouts, the transfer zone at a crossing nose in complex turnout  
112 system still imposes high-frequency forces to track components. Generally, the turnout bearers for  
113 supporting points and crossing structures were designed using the beam on elastic foundation  
114 analysis or 2-D FE grillage modelling (Manalo et al., 2012). Kaewunruen (2014a; 2014b) indicated  
115 from recent authority work that some additional factors were often neglected from the grillage  
116 analyses, although they must be taken into account, including:

- 117 • Extra length of turnout bearers in comparison with standard sleepers
- 118 • Centrifugal forces through curved pairs of rails
- 119 • Forces and bending moments induced from points motors and other signaling equipment
- 120 • Impact forces induced by wheel-rail interaction
- 121 • Mechanical rail joints.

122 This investigation arose from an emerging risk of broken concrete bearers on a mixed-  
123 traffics line in New South Wales (NSW), Australia. Due to the complexity of the loadings and  
124 damage modes in railway turnouts, this study aims to establish a three dimensional (3D) Finite-  
125 element (FE) model. The 3D FE model will adopts an elasto-plastic region of bending and shear  
126 deformation of materials. The 3D FE model was developed based upon a common tangential  
127 turnout used in Australia. The finding confirms that the crossing panel is where turnout bearers  
128 experience the greatest bending moment and shear force (Iwinicki et al., 2009). Despite a large  
129 number of investigations, there exists no report on torsional effect on damages of turnout

130 components in the real world (Sae Siew et al., 2015). A highlight of this study is the torsional effect  
131 on the turnout structure where improved resiliency will help suppress such an important effect  
132 (Kaewunruen, 2012, 2014c; Nimbalkar et al., 2012). The findings will enhance public safety in  
133 railway networks with turnouts and crossings.

134

### 135 **Finite Element (FE) Modelling**

136 A previous research carried out by Manalo et al. (2010, 2012) analysed the turnout system  
137 utilising a grillage beam method. The research was carried out taking in consideration the build and  
138 specification of rail used in Queensland, Australia. Results obtained in the study showed that the  
139 maximum bending moment and shear force can be witnessed within the switch panel. The results  
140 using the grillage beam method seem to have discrepancies with the field observations where the  
141 maximum bending and shear forces were evident within the crossing panel (Kaewunruen, 2012). A  
142 number of research has been conducted to locate the critical section within a turnout, and many of  
143 which conclude upon the critical section being located specifically at the crossing panel (Kassa and  
144 Nielsen, 2009; Wiest et al., 2008a; Xiao et al., 2011).

145 This paper presents the 3D FE analysis using ABAQUS<sup>®</sup> considering the whole turnout  
146 which fully comprises of sleepers, rail, guard rails, crossing nose, rail pads, baseplates and guardrail  
147 support plates. The benefits of modelling in 3D are to incorporate the effects of the neighbouring  
148 sleepers and to take in consideration the longitudinal forces of the continual rail. The boundary  
149 conditions of the central 3D model can be simulated enabling vibrations to radiate beyond the  
150 model (Karlsson and Sorensen, 2006).

### 151 ***Wheel/rail interface (W-R)***

152 General track design is based upon the consideration of static axle loads, total sum of axle  
153 loads, and running speeds of vehicles as dependant variables. The standard also specifies that  
154 vertical static forces are to be designed to accommodate for the combined loading of static wheels,  
155 wheel diameters and wheel tread profiles, and for these loading to not jeopardise the safety of the

156 track system by causing excessive stresses and deformation under all normal track conditions.  
 157 Andersson and Dahlberg (1998) established a linear FE model with modal damping that focuses on  
 158 the vertical dynamics of a train passing through a turnout. Results showed that the rail discontinuity  
 159 causes an impact increase between wheel and rail, referred to as a ‘jump’. The condition of the  
 160 wheel and rail greatly influences the W-R contact force, for the greater the irregularities, the larger  
 161 the contact force produced. The greater contact force will accelerate the wear and/or crack growth  
 162 rate in the turnout crossing. Sun et al. (2010) provided an insight on the potential sites for impact  
 163 and fatigue damage as the train wheel traverses through the nose of the crossing. Firstly, the wing  
 164 rail fatigue damage is caused by contact from the far side of wheel. Secondly, the transition of the  
 165 wheel between the wing rail and nose causes a dipping movement. This is due to the tracking on the  
 166 wing rail to an upward motion on the ramp of the nose resulting in fatigue damage. Greater contact  
 167 stress can be seen due to the acute contact area in the crossing nose. It is noteworthy that the  
 168 crossing process will only force the wheel in contact to dip. The British Railways Board  
 169 (Cherkashin et al., 2009) expressed that the permissible track forces ( $P_2$ ) for railway vehicles  
 170 negotiating a discontinuity in rail profile to not exceed 322 kN whilst operating at its maximum  
 171 design speed. The  $P_2$  force is calculated using the following formula:

$$P_2 = Q + (A_z \cdot V_m \cdot M \cdot C \cdot K) \quad (1)$$

Where

$$M = \left[ \frac{M_v}{M_v + M_z} \right]^{0.5} \quad (2)$$

$$M = \left[ \frac{M_v}{M_v + M_z} \right]$$

$$C = \left[ \frac{\pi \cdot C_z}{4[K_z(M_v + M_z)]^{0.5}} \right] \quad (3)$$

$$K = (K_z \cdot M_v)^{0.5} \quad (4)$$

the lesser of  $Q = 0.13D \times 10^3$  or  $Q = 125 \times 10^3$  (5)

172 Where  $D$  is the wheel diameter (mm),  $Q$  is the maximum static wheel load (N),  $V_m$  is the maximum  
 173 normal operating speed (m/s),  $M_v$  is the effective vertical unsprung mass per wheel (kg),  $A_z$  is total  
 174 angle of vertical ramp discontinuity taken as 0.02 rad,  $M_z$  taken as 245 kg as the effective vertical

175 rail mass per wheel,  $C_z$  taken as  $55.4 \times 10^3$  N/m as the effective vertical rail damping rate per wheel  
176 and  $K_z$  taken as  $62 \times 10^6$  N/m as the effective vertical rail stiffness per wheel.

177 Lateral forces are designed as to not jeopardise the structural integrity of the rail and track.  
178 Unless supported by appropriate technical justification, vehicles attempting to negotiate a lateral  
179 ramp discontinuity in track alignment, when travelling on a curve at maximum normal operating  
180 speed and at maximum cant deficiency, without exceeding a total lateral force level per axles of 71  
181 kN, and is to be calculated using the following formula:

$$Y = W \cdot A_d + A_y \cdot V_m \left[ \frac{M_u}{M_u + M_y} \right]^{0.5} \cdot [K_y \cdot M_u]^{0.5} \quad (6)$$

182 Where  $Y$  is the lateral force per axle (N),  $W$  is the static axle load (N),  $A_d$  is the maximum  
183 normal operating cant deficiency angle (rad),  $V_m$  is the maximum normal operating speed (m/s),  $M_u$   
184 is the effective lateral unsprung mass per axle (kg),  $A_y$  is taken to be 0.0038 rad which is the angle  
185 of lateral ramp discontinuity,  $M_y$  taken as 170 kg and is the effective lateral rail mass per wheel and  
186  $K_y$  taken as  $25 \times 10^6$  N/m as the effective lateral rail stiffness per wheel.

### 187 ***Turnout Components***

188 The FE model comprises of entirely 3D deformable solids; straight and curved rail, sleepers  
189 of varying length and a ballast layer as the track support. This study focuses on the behaviour of the  
190 sleeper and ballast; therefore, a suitably accurate rail seat load within a tangential configuration is  
191 required for the analysis. Steel rails were modelled in 3D to account for its cross sectional  
192 properties, the width of the contact patch between the wheel and rail, the width of the rail web and  
193 the width of the rail footing. The rail and switch rail profiles were validated against rail authority's  
194 specifications (RailCorp, 2012a, 2012b, 2012c). Concrete bearers have been modelled as  
195 rectangular blocks with dimensions nominated according to the specifications varying lengths  
196 between 2.5 m to 7.5 m according to the turnout design as tabulated in Table 1.

197 The elastic modulus of steel rails and crossing is defined by the initial slope of the stress-  
198 strain relationship to the extent of the upper yield threshold, as illustrated in Figure 2. For concrete  
199 material, it is assumed that its compressive stress behaviour is to be linear given that it does not



200 exceed  $0.4f'_c$ . Beyond the linear threshold, stress is expressed as a function of strain accordingly to  
 201 Equation (7). A graphical representation of the stress-strain relationship of concrete is depicted in  
 202 Figure 3.

$$\sigma_c = \frac{f'_c \gamma (\varepsilon_c / \varepsilon'_c)}{\gamma - 1 + (\varepsilon_c / \varepsilon'_c)^\gamma} \quad (7)$$

where  $\gamma = \left| \frac{f'_c}{32.4} \right|^3 + 1.55$  and  $\varepsilon'_c = 0.002$  (8)

203 Indraratna and Nimbalkar (2011) proposed an idealisation of the ballast layer as a  
 204 hardening-soil (HS) model. This method is an advanced method in analysing the mechanical  
 205 behaviour in soil as it considers the plasticity theory, along with the effect of viscosity on the shear  
 206 strain and a yield cap. Because this analysis focuses mostly on an elastic range, the evaluation takes  
 207 upon the approach of simplifying the ballasted track support using elastic solid elements. A track  
 208 support modulus of 50 MPa is adopted to comply with the design requirements and field data  
 209 (RailCorp, 2012a, 2012b).

### 210 ***Boundary Conditions***

211 A sensitivity analyses has been undertaken for mesh sizes for each rail components. As the  
 212 mesh sizes and the material densities are different between the two tied objects, a tie constraint is  
 213 generated to allow for ABAQUS<sup>®</sup> to automatically optimise and refine the interface mesh. Tie  
 214 constraints are applied to the rail and the concrete sleepers to represent the rail fastener. Instead of  
 215 frictional interaction and the effect of submersed sleepers in a ballast layer, the sleepers are tied  
 216 onto the underlying ballast layer to greatly reduce computational effort. As all members are tied,  
 217 translational and rotational degrees of freedom will be equal throughout. All tie constraints will be  
 218 taken to be surface to surface, as opposed to a simplified node to surface, as this will allow for  
 219 uniform distribution between the tied components (Karlsson and Sorensen, 2006).

220 A fixed boundary condition is applied to the bottom most surface of the ballast to idealise  
 221 the substructure and a symmetrical constraint is applied to the ends of the rail to idealise a

222 continuous rail within the relevant plane, in this case the Z-axis. The sleepers are attached to other  
223 members with boundary constraints, and they can deform freely with the ballast bed.

224

### 225 ***Load Conditions***

226 The FE model predicts the behaviour of the turnout by considering multi-wheel impacts  
227 which would simulate in-service and cyclic loading, and will be adapted as a set of concentrated  
228 loads negotiating the turnout to represent a moving coupled locomotive. Loading configuration is in  
229 accordance with Standards Australia (2004), using the contact position to generate the maximum  
230 impact force. Design loads can be depicted in Figure 4a, which simulate the worst case loading  
231 configuration that can be exerted onto a rail track. The coupled locomotive is simulated with four  
232 300 kN axle loads and a single 360 kN axle load 2 meters ahead of the group.

233 The above load set is applied to the model at 600mm increments, or referred hereafter as  
234 load sets. A total of 48 load steps (including model initiation) have been modelled to generate the  
235 overall movement of the locomotive negotiating the turnout. Figure 4b illustrates loading  
236 configurations for particular steps.

### 237 ***Validation***

238 The deflection of the sleeper is dependent on the mesh sizes of the ballast; the ballast serves  
239 as a slave surface in which the sleeper is modelled to suppress into. Along with an accurate resultant  
240 deflection, the time required to compute the analysis is also significant in selecting an optimum  
241 mesh size. It is noted that the typical aggregate size of ballast is anywhere between 13 mm to 65  
242 mm (RailCorp, 2012a). An initial analysis was carried out to determine the maximum deflection  
243 under the said design train loading. A mesh size of 80 mm x 80 mm had been nominated. Figure 5  
244 below shows the maximum vertical deflection, taken at the mid-point of each sleeper, with a single  
245 pass of the coupled locomotive load. The results show that sleeper number 47 (out of a total of 51  
246 sleepers), which is located directly underneath the crossing nose, is subjected to the greatest  
247 deflection. The next step in analysing the sleeper behaviour would be to assess the deflection in

248 relations to the location of the load, in this case as a function of load step. The deflection response is  
249 presented graphically in Figure 6. It can be seen that the sleeper does not undergo any translations  
250 up until the 35<sup>th</sup> load step. This is an important step in dramatically reducing the computational time  
251 required to analyse the model with different mesh sizes. As we had located the critical sleeper in the  
252 preliminary test, it is advantageous to exclude all previous steps between the initial and 34<sup>th</sup> step  
253 from the analysis in determining optimum mesh size as this will reduce the computational time by  
254 almost 80%. Table 2 lists the maximum deflection of the chosen sleeper under train loading  
255 according to varied mesh sizes and Figure 7 depicts the critical response between load steps 35 to  
256 47.

257 It can be seen from the results above that the change in the mesh size does not significantly  
258 affect the maximum deflection as seen by the largest deviation ( $< 0.3$  mm) that is negligible. As  
259 previously mentioned, computational time is taken into great consideration, and it can be seen that  
260 although the 60 mm and 100 mm mesh yield the same result, the former takes almost 4.5 times the  
261 amount of time to compute compared to the latter. Given this, the 100 mm x 100 mm mesh will be  
262 accurate and the most efficient for this study purpose. Note that the track stiffness of this model has  
263 been benchmarked with the field measurement (Sae Siew et al., 2015).

264

## 265 **Results and Discussion**

266 Field observations suggested that impacts at turnout crossing frequently cause the most  
267 maintenance of supporting bearers and fastening systems. These impacts are due to the wheel rail  
268 interaction over the transfer zone (Kaewunruen, 2014a, 2014b). The FE model, which has been  
269 developed to simulate a turnout system subjected to a moving design load, reveals similar results. It  
270 is found that the sleepers, which undergo the greatest deflection of a coupled locomotive pass, are  
271 the sleepers underneath the crossing nose (maximum at sleeper #47). The sensitivity analysis  
272 illustrates the maximum deflection in all sleepers with the passing of a moving couple train load,  
273 300LA (Standards Australia, 2004). From this analysis, it can be seen from Figure 8 that sleeper 47

274 experiences the greatest deflection, with a resultant of 2.54 mm. Figure 9 illustrates the deflection  
275 response of the critical sleeper (47) in terms of the location of train, or load step. The sharp spike in  
276 deflection clearly defines the moment at which each wheel axle impacts the above rail, in this case  
277 the crossing nose.

278 The direction of translations is also an important factor, especially when predicting the long-  
279 term stability of the ballast layer. It can be seen from the deflection shapes depicted in Figures 10  
280 and 11 that the translation are not vertical, and tend to suggest the whole movement of the sleeper to  
281 be a rotation or a twist.

282 Figure 12 further explores the effects of the sleeper deflection into the underlying ballast  
283 layer. The below deflection is a resultant of 300LA loading (Standards Australia, 2004) as the front  
284 axle impacts the crossing nose, to then exit the turnout on the diverging track. The stress parameters  
285 are calculated based on the Von Mises yield criterion, which was explained in earlier section.  
286 Examples of the shear stress distribution for a particular load step along the turnout system are  
287 detailed below in Figure 13. Shear stress within this particular model is about the XY plane,  $S_{12}$ ,  
288 or  $\sigma_{12}$ . The resultant stresses are based upon critical loading configuration. It is found that the  
289 sleeper, which experiences the greatest shear and bending moment, is found to be the one directly  
290 underneath the crossing nose (sleeper 47). It is important to note that torsional behaviour observed  
291 is likely caused by the crossing angle, which influences wheel/rail contact path and the loading  
292 location.

293 The critical sleepers within the specified length have been chosen accordingly to the  
294 maximum resultant deflection during one passing of a moving load. The largest deflection in a  
295 sleeper of lengths 2.6-2.8 metres has been recorded within sleeper 21 (sleeper right underneath the  
296 heel joint), resulting in a maximum deflection of 1.28 mm. The largest deflection recorded within  
297 the range of 2.801-5.200 metres has been established earlier as the critical sleeper, sleeper 47. The  
298 maximum deflection values are generated using the sleeper deflection with relation to the load  
299 steps. Critical loading occurs during load step 36 for sleeper 47 (sleeper right underneath the

300 crossing during the passage of a running wheel), and load step 18 for sleeper 21 (sleeper right  
301 underneath the heel joint during the rapid change of train direction).

302

### 303 **Conclusions**

304 This paper presents a part of the investigation that is arisen from the field observations and  
305 measurements on a mixed traffic rail line where broken concrete bearers and loosen fasteners were  
306 reported routinely. A 3D FE model has been established for the analysis of a complete turnout  
307 system. The primary objective of this study was to determine the critical location; be able to realise  
308 the critical deflection, and validate shear force and bending moment envelopes of a turnout system.  
309 To address this, ABAQUS® was employed to carry out all modelling and post-processing of a  
310 complete 3D turnout.

311 Through the sensitivity analysis, it is clear that turnout bearers right underneath crossing  
312 panel experience the highest load actions, resulting in the largest deformations. Importantly, we are  
313 the first to report that the cute angle of crossing nose also induces torsional force on the supporting  
314 track structure. Although the torsion can be coped with by the ballast aggregates, such an effect  
315 causes damages to fastening systems and the bearers as evidenced in practice. Future work will  
316 evaluate the effects of dimension, topology and stiffness of fastening systems to mitigate the  
317 torsional crossing impacts.

318

### 319 **Acknowledgement**

320 The authors are grateful to University of Western Sydney and RailCorp for the support  
321 throughout this study. Also, the third author wishes to thank Australian Government for his  
322 Endeavour Executive Fellowships at Massachusetts Institute of Technology, Harvard University,  
323 and Chalmers University of Technology.

324

325

326

327 **References**

- 328  
329 Andersson, C. and Dahlberg, T. 1998. Wheel/rail impacts at a railway turnout crossing.  
330 *Proceedings of the Institution of Mechanical Engineers*, 212, 123-134.
- 331 Cherkashin, U., Zakharov, S. & Semechkin, A. 2009. An overview of rolling stock and track  
332 monitoring systems and guidelines to provide safety of heavy and long train operation in the  
333 Russian Railways. *Proceedings of the Institution of Mechanical Engineers, Part F: Journal of*  
334 *Rail and Rapid Transit*, 223, 199-208.
- 335 Esveld, C., 2001. *Modern Railway Track*, The Netherlands MRT Press.
- 336 Indraratna, B. & Nimbalkar, S. 2011. Implications of ballast breakage on ballasted railway track  
337 based on numerical modelling.
- 338 Iwnicki, S., Bezin, Y., Xie, G. & Kassa, E. 2009. Advances in vehicle-track interaction tools.  
339 *Railway Gazette International*, 165, 47-49,51-52.
- 340 Kaewunruen, S. 2007. Experimental and numerical studies for evaluating dynamic behaviour of  
341 prestressed concrete sleepers subject to severe impact loading. *PhD Thesis*, School of Civil,  
342 Mining, and Environmental Engineering, University of Wollongong, Australia.
- 343 Kaewunruen, S. 2012. Effectiveness of using elastomeric pads to mitigate impact vibration at an  
344 urban turnout crossing, in Maeda et al. (Eds.) *Noise and Vibration Mitigation for Rail*  
345 *Transportation Systems*, Springer, 357-365.
- 346 Kaewunruen, S. 2014a, "Monitoring structural deterioration of railway turnout systems via dynamic  
347 wheel/rail interaction." *Case Studies in Non-destructive Testing and Evaluation*, in press.
- 348 Kaewunruen, S. 2014b, "Monitoring in-service performance of fibre-reinforced foamed urethane  
349 material as timber-replacement sleepers/bearers in railway urban turnout systems." *Structural*  
350 *Monitoring & Maintenance*, 1(1): 131-157 (invited).
- 351 Kaewunruen, S. 2014c, "Discussion of 'Mitigation of Ground Vibration Generated by High-Speed  
352 Trains on Saturated Poroelastic Ground with Under-Sleeper Pads?.'" *ASCE Journal of*  
353 *Transportation Engineering*, in press.
- 354 Kaewunruen, S. & Remennikov, A. M. 2006. Sensitivity analysis of free vibration characteristics of  
355 an in situ railway concrete sleeper to variations of rail pad parameters. *Journal of Sound and*  
356 *Vibration*, 298, 453-461.
- 357 Kaewunruen, S. & Remennikov, A. M. 2007. Investigation of free vibrations of voided concrete  
358 sleepers in railway track system. *Proceedings of the Institution of Mechanical Engineers*, 221,  
359 495-507.

360 Kaewunruen, S. and Remennikov, A.M., 2008, Nonlinear transient analysis of railway concrete  
361 sleepers in track systems. *International Journal of Structural Stability and Dynamics*, 8(3):  
362 505-520.

363 Kaewunruen, S. and Remennikov, A.M., 2009a, "Progressive impact behaviours of prestressed  
364 concrete sleepers in railway track environments." *Engineering Structures*, 31(10):2460-2473.

365 Kaewunruen, S. and Remennikov, A.M., 2009b, "Impact fatigue responses of pre-stressed concrete  
366 sleepers in railway track systems." *The IES Journal Part A: Civil & Structural Engineering*, 2  
367 (1), 47-58.

368 Kaewunruen, S. and Remennikov, A.M., 2010, "Dynamic crack propagations of prestressed  
369 concrete sleepers in railway track systems subjected to severe impact loads." *ASCE Journal of*  
370 *Structural Engineering*, 136(6): 749-754.

371 Kaewunruen, S. and Remennikov, A.M., 2013, "On the residual energy toughness of prestressed  
372 concrete sleepers in railway track structures subjected to repeated impact loads." *Electronic*  
373 *Journal of Structural Engineering*, 13(1): 31-47.

374 Kaewunruen, S., Remennikov, A.M., Aikawa, A., and Sakai, H., 2014, "Free vibrations of  
375 interspersed railway track systems in three-dimensional space." *Acoustics Australia*, 42(1): 20-  
376 26.

377 Karlsson and Sorensen 2006. *ABAQUS/CAE User's Manual: Element*, Pawtucket, Rhode Island,  
378 Hibbitt Publication.

379 Kassa, E. & Nielsen, J. 2008a. Dynamic interaction between train and railway turnout: full-scale  
380 field test and validation of simulation models. *Vehicle System Dynamics*, 46, 521-534.

381 Kassa, E. & Nielsen, J. C. O. 2008b. Stochastic analysis of dynamic interaction between train and  
382 railway turnout. *Vehicle System Dynamics*, 46, 429-449.

383 Kassa, E. & Nielsen, J. C. O. 2009. Dynamic train–turnout interaction in an extended frequency  
384 range using a detailed model of track dynamics. *Journal of Sound and Vibration*, 320, 893-914.

385 Manalo, A., Aravinthan, T., Karunasena, W. & Stevens, N. 2012. Analysis of a typical railway  
386 turnout sleeper system using grillage beam analogy. *Finite Elements in Analysis & Design*, 48,  
387 1376.

388 Nimbalkar, S., Indraratna, B., Dash, S. & Christie, D. 2012. Improved Performance of Railway  
389 Ballast under Impact Loads Using Shock Mats. *Journal of Geotechnical and Geoenvironmental*  
390 *Engineering*, 138, 281-294.

391 Railcorp Nsw 2012a. ESC 240. *Ballast*. Rail Corporation of New South Wales.

392 Railcorp Nsw 2012b. ESC 250. *Turnouts and special trackwork*. Rail Corporation of New South  
393 Wales.

394 Railcorp Nsw 2012c. SPC 233. *Concrete turnout bearers*. Rail Corporation of New South Wales.  
395 Remennikov, A. M. & Kaewunruen, S. 2008. A review of loading conditions for railway track  
396 structures due to train and track vertical interaction. *Structural Control and Health Monitoring*,  
397 15(2), 207-234.  
398 Sae Siew, J., Mirza, O., Kaewunruen, S. 2015. Nonlinear finite element modelling of railway  
399 turnout system considering bearer/sleeper-ballast interaction. *Journal of Structures*, ID 598562,  
400 <http://dx.doi.org/10.1155/2015/598562>  
401 Standards Australia 2002. AS 1085.1. *Railway track material - Steel rails*. Standards Australia.  
402 Standards Australia 2004. AS 5100.2. *Bridge design - Design loads*. Standards Australia.  
403 Sun, Y. Q., Cole, C. & Mcclanachan, M. 2010. The calculation of wheel impact force due to the  
404 interaction between vehicle and a turnout. *Proceedings of the Institution of Mechanical*  
405 *Engineers*, 224, 391-403.  
406 Wiest, M., Daves, W., Fischer, F. D. & Ossberger, H. 2008a. Deformation and damage of a crossing  
407 nose due to wheel passages. *Wear*, 265, 1431-1438.  
408 Wiest, M., Kassa, E., Daves, W., Nielsen, J. C. O. & Ossberger, H. 2008b. Assessment of methods  
409 for calculating contact pressure in wheel-rail/switch contact. *Wear*, 265, 1439-1445.  
410 Xiao, J., Zhang, F. & Qian, L. 2011. Numerical simulation of stress and deformation in a railway  
411 crossing. *Engineering Failure Analysis*, 18, 2296-2304.

412

413

414

415

416

417

418

419

420

421

422



423

## List of Figures

424 Figure 1. Typical components of a railway turnout (after Kaewunruen, 2014a).

Figure 2. Stress-strain relationship of structural steel

425 Figure 3. Stress-strain relationship of concrete

426 Figure 4. Railway Traffic Loads - Axle Loads

427 Figure 5. Mid-point deflections of each sleeper along the turnout

428 Figure 6. Displacement envelope of the sleeper right underneath the crossing (#47)

429 Figure 7. Effect of mesh sizes on the deflection of the sleeper right underneath the crossing (#47)

Figure 8. Maximum deflection of sleepers 1-51 under applied moving load

430 Figure 9. Deflection of critical sleeper (47) in relation to location of load

431 Figure 10. Deflection mode of critical sleeper - XY plane

432 Figure 11. Deflection mode of critical sleeper – 3D plane centre cut view

433 Figure 12. Deflections of ballast layer

434 Figure 13. Shear stresses of turnout sleepers

435

436

437 **Table 1.** Design properties of materials

Materials	Elastic modulus (MPa)	Compressive strength (MPa)	Tensile strength (MPa)
Concrete	38,000	36 - 55	4.0 - 6.30
Prestressing tendon	200,000	-	1,700
Steel rails	205,000	-	-

438

439

440

441

442

443

444

445

446

447

448

449

450

451

452

453

454

455

456

457

458

459

460

461

462

463

464

465

466

467

468

469

470

471

472

473

474

475

**Table 2** Resultant deflection of sleeper 47 and computational time with varying ballast mesh size

<b>Mesh size (mm)</b>	<b>Deflection (mm)</b>	<b>Computational time (s)</b>
60 x 60	2.54	24,784
70 x 70	2.32	12,638
80 x 80	2.28	10,824
90 x 90	2.59	5,655
100 x 100	2.54	5,547

476

477

478

479

480

481

482

483

484

485

486

487

488

489

490

491

492

493

494

495

496

497

498

499

500

501

502

503

504

505

506

507

508

509

510

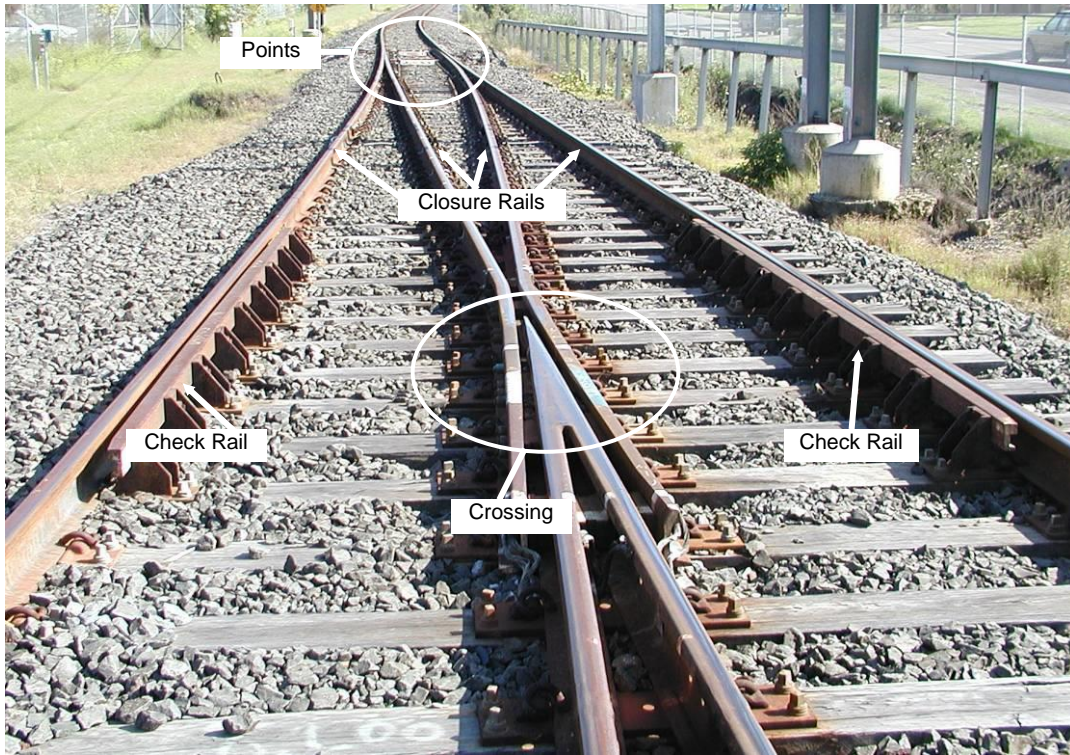
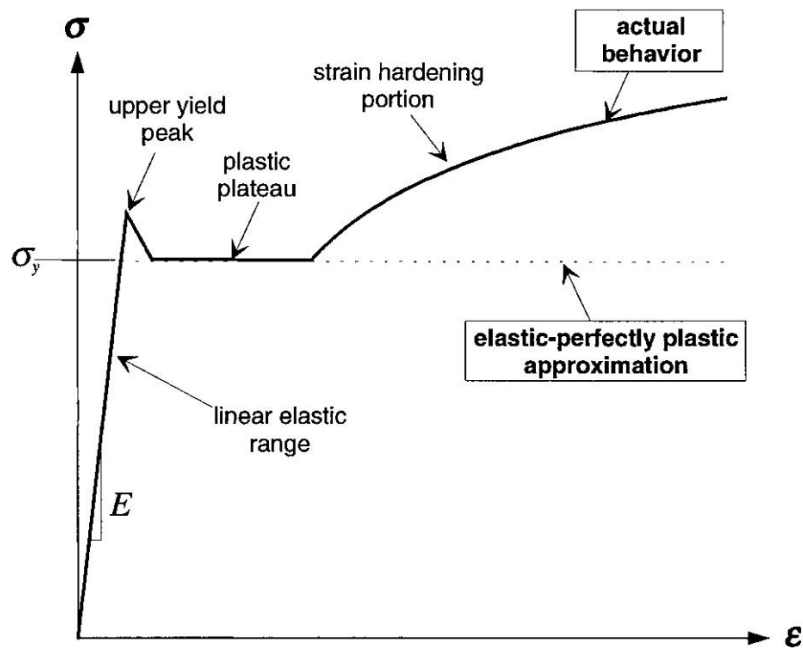


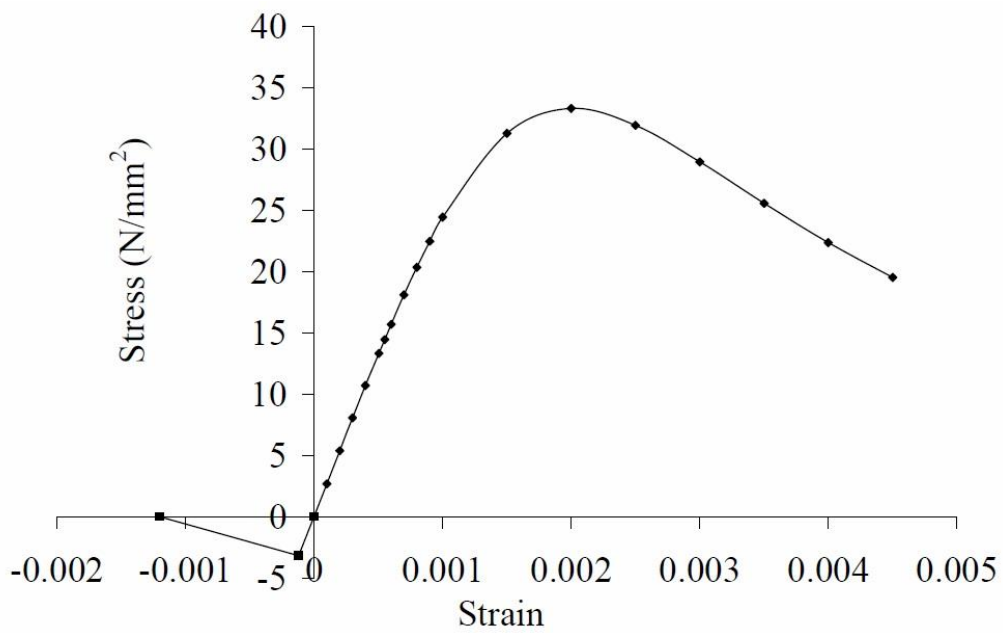
**Figure 1.** Typical components of a railway turnout (after Kaewunruen, 2014a).

512  
513  
514  
515  
516  
517  
518  
519  
520  
521  
522  
523  
524  
525  
526  
527  
528  
529  
530  
531  
532  
533  
534



535

**Figure 2.** Stress-strain relationship of structural steel



536

537

538

539

540

541

542

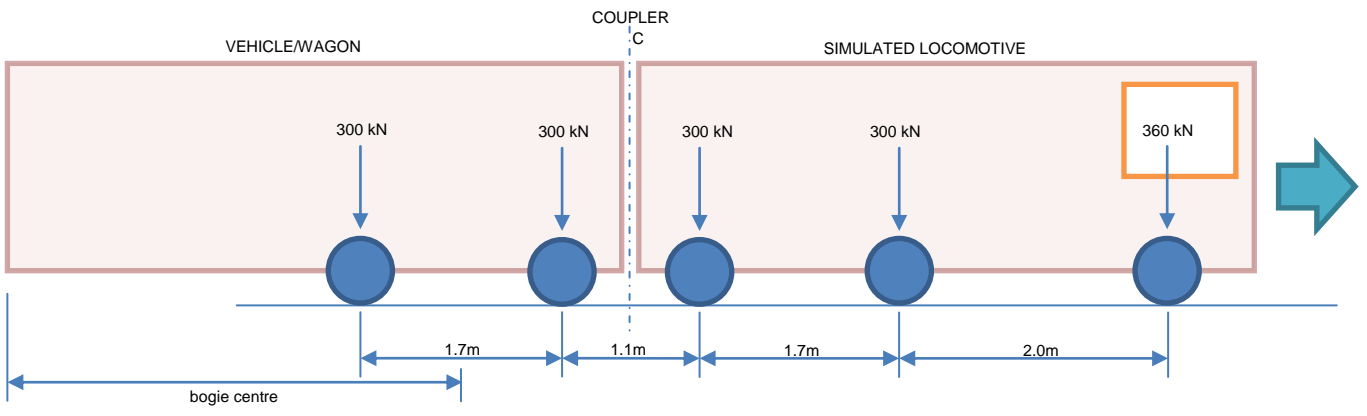
543

544

545

**Figure 3.** Stress-strain relationship of concrete

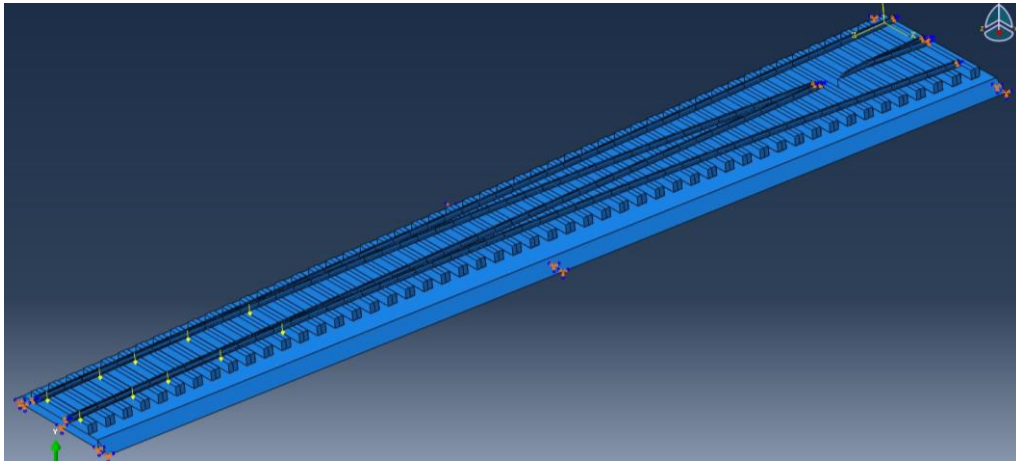
546  
547  
548  
549  
550  
551  
552  
553  
554  
555  
556  
557  
558  
559  
560  
561  
562  
563  
564  
565  
566  
567  
568  
569  
570  
571



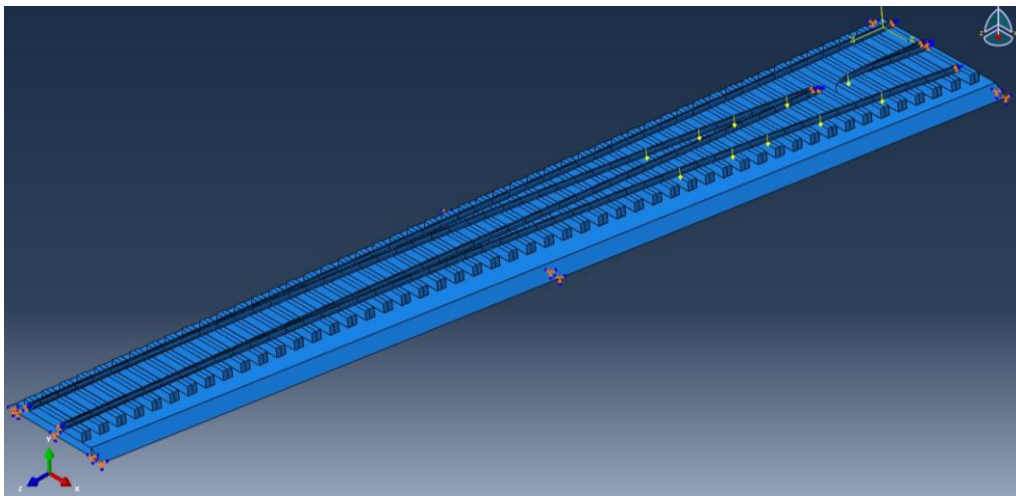
a) 300LA Load case

**Figure 4.** Railway Traffic Loads - Axle Loads

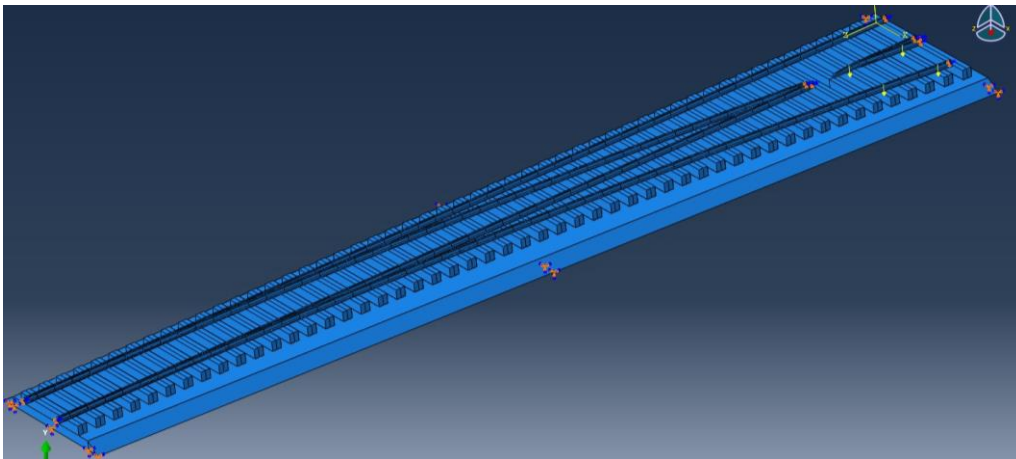
572



573  
574



575  
576



577  
578

b) Load steps: 300LA coupled locomotive design loading on turnout; (top) load step 2, (middle) load step 36 and (bottom) load step 48

**Figure 4.** Railway Traffic Loads - Axle Loads

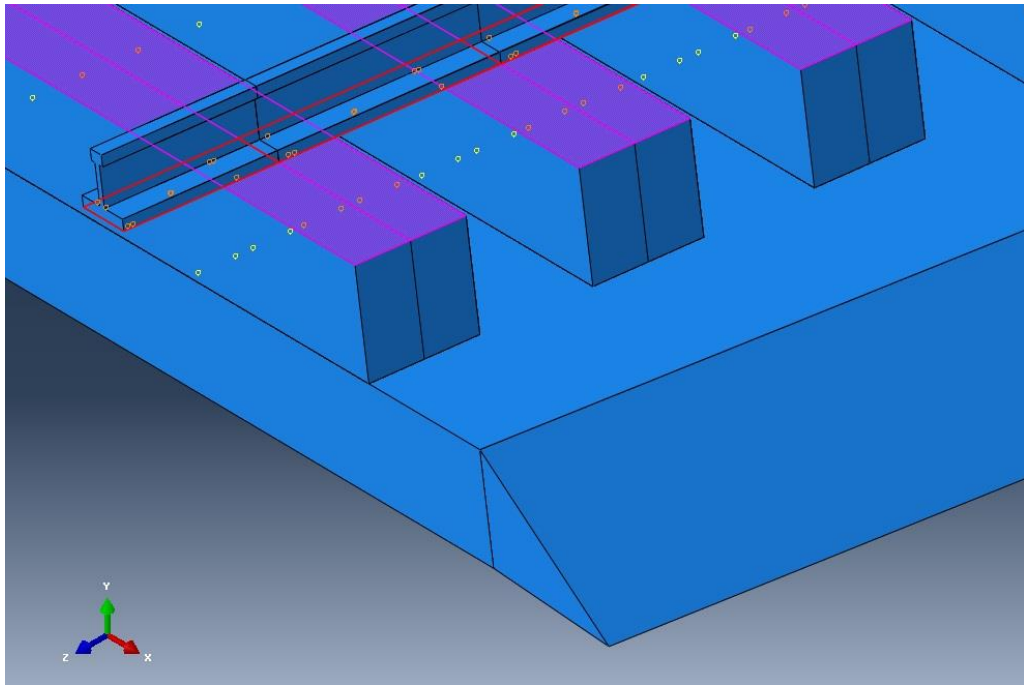
579

580

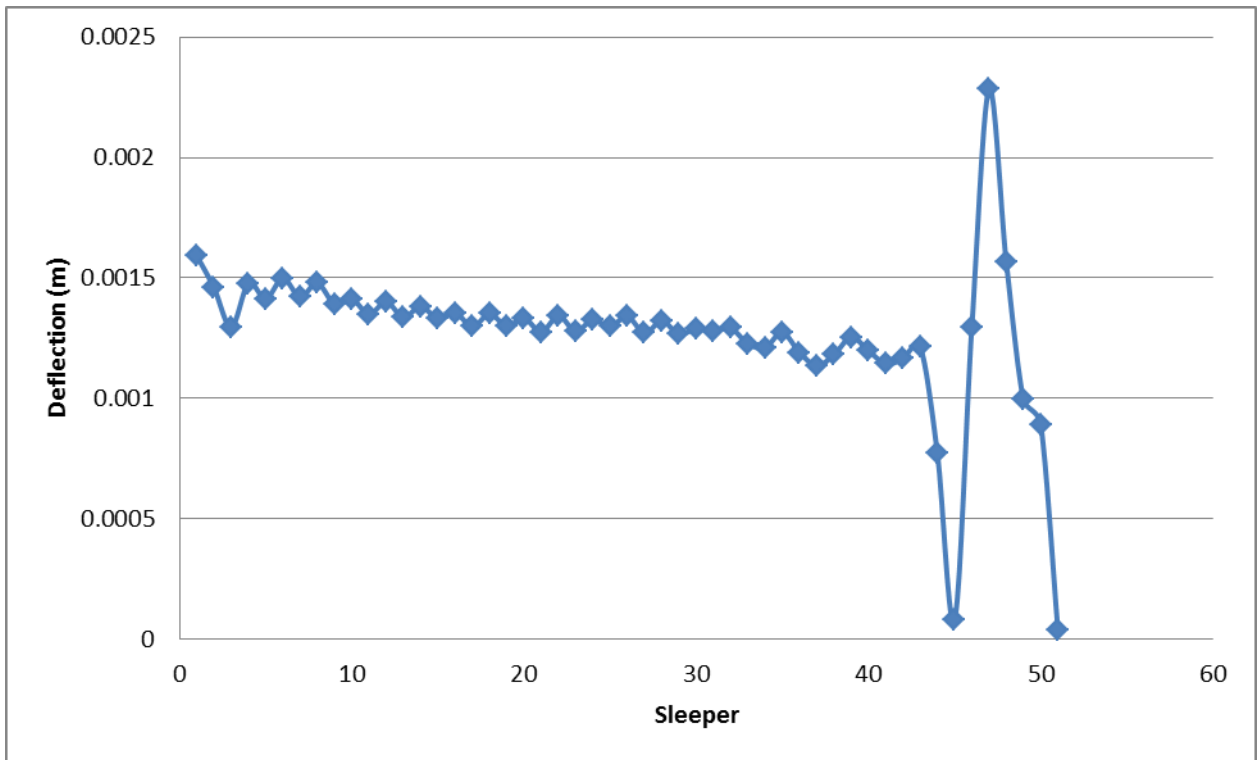
581

582

583



a) Tie constraint between rail and sleeper

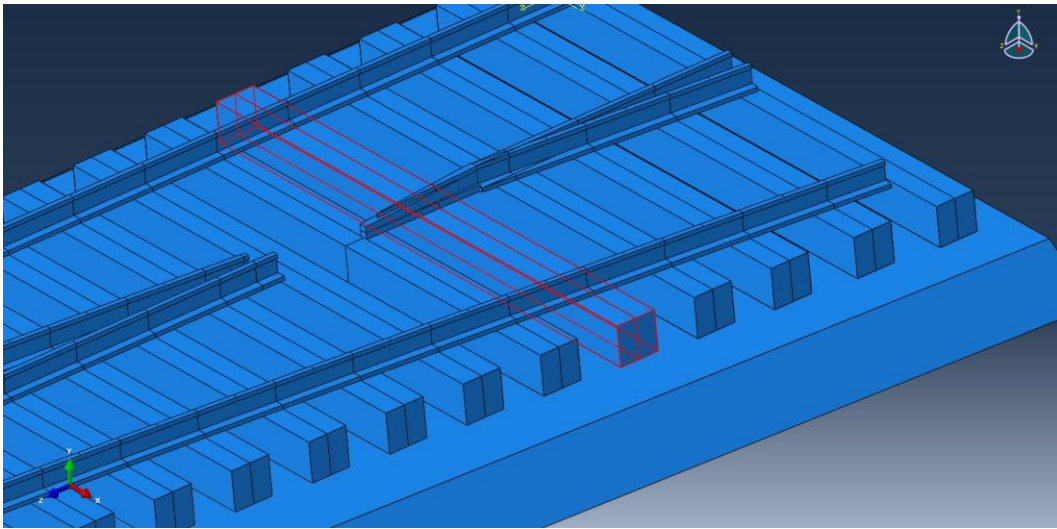


b) Maximum recorded deflection at each sleeper (mid-point)

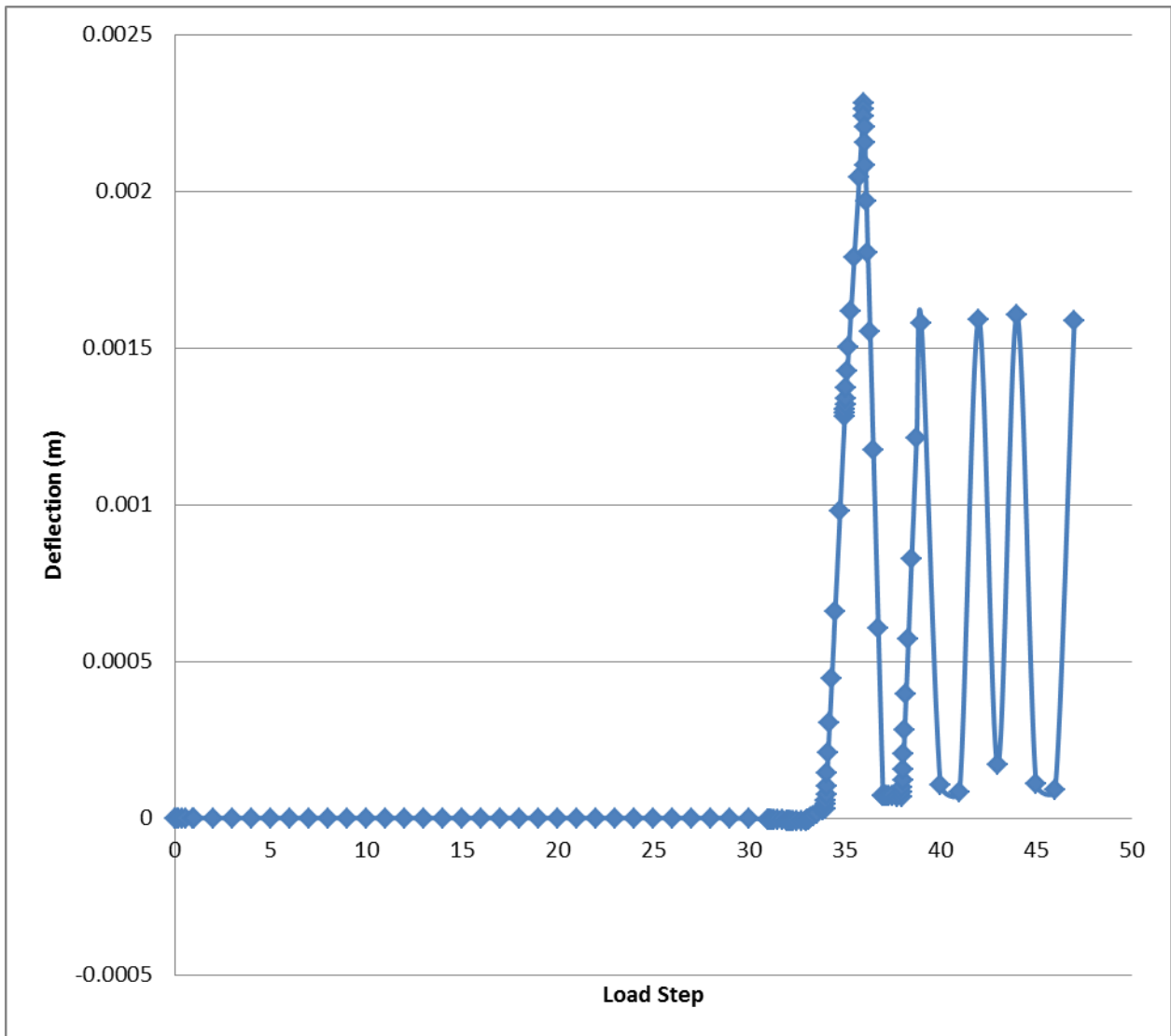
**Figure 5.** Mid-point deflections of each sleeper along the turnout



588



a) Sleeper 47 (red) experiences the greatest deflection



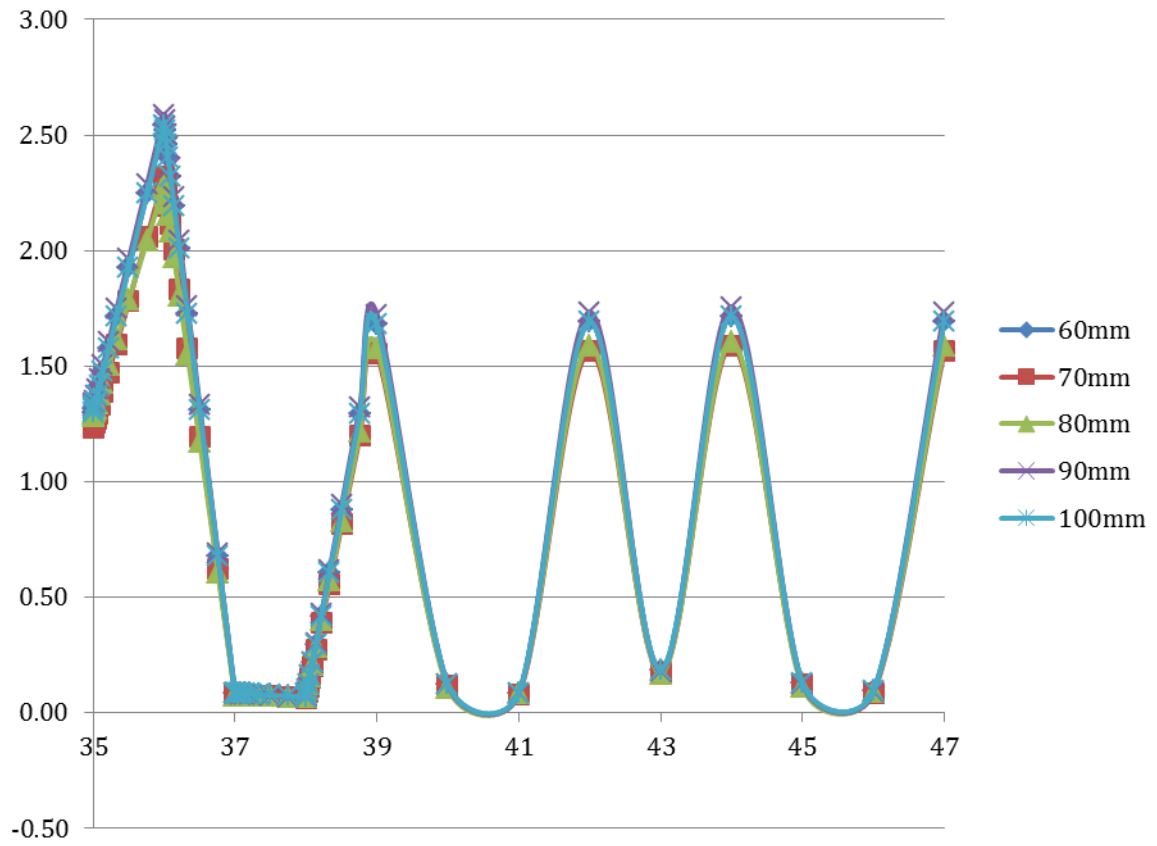
589

b) Deflection response of Sleeper 47 at each load step

590

591

**Figure 6.** Displacement envelope of the sleeper right underneath the crossing (#47)



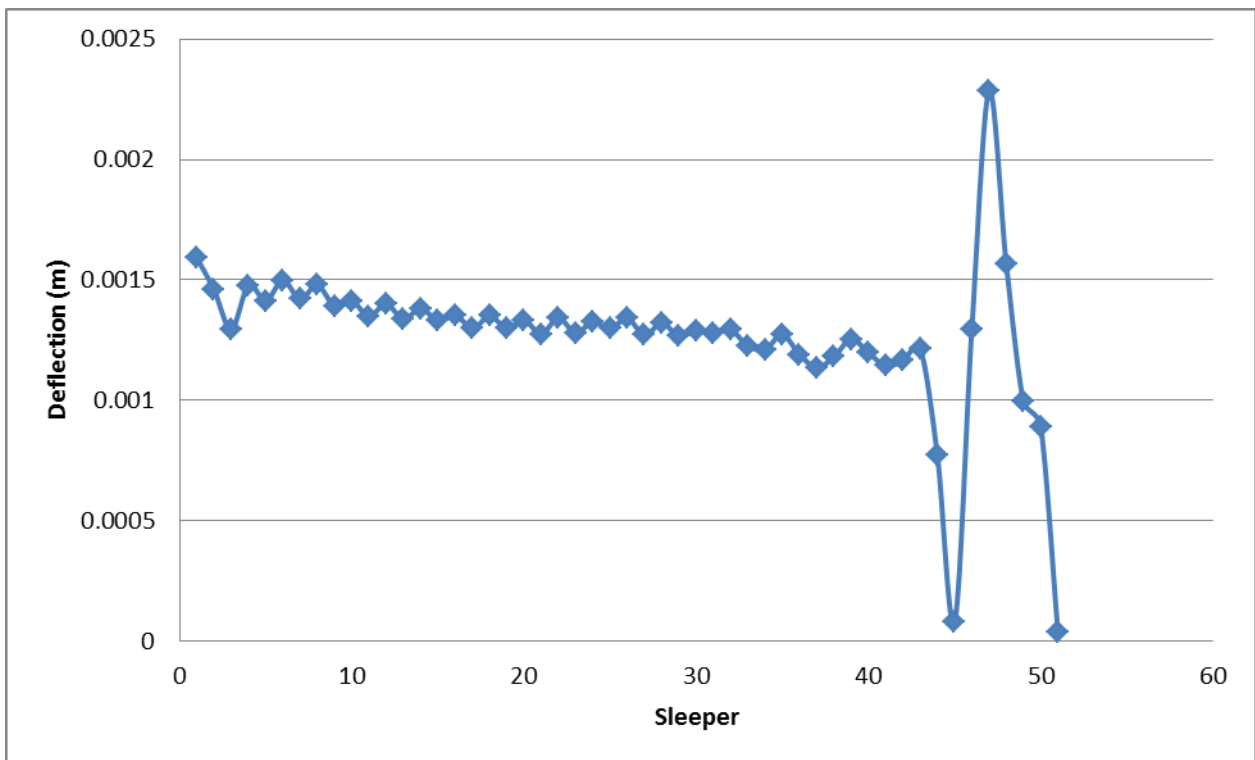
592

**Figure 7** Effect of mesh sizes on the deflection of the sleeper right underneath the crossing (#47)

593

594

595



596

**Figure 8** Maximum deflection of sleepers 1-51 under applied moving load

597

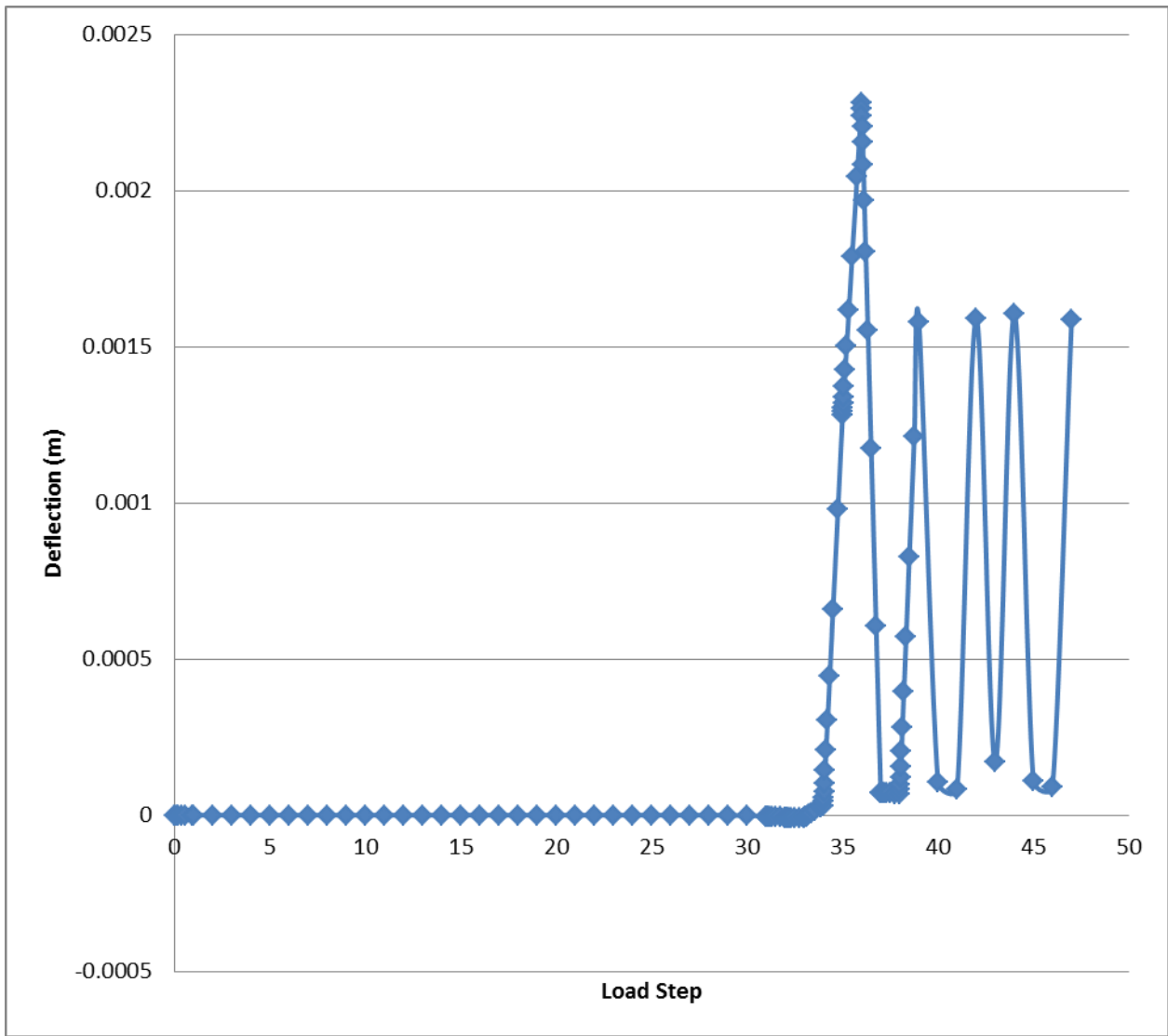


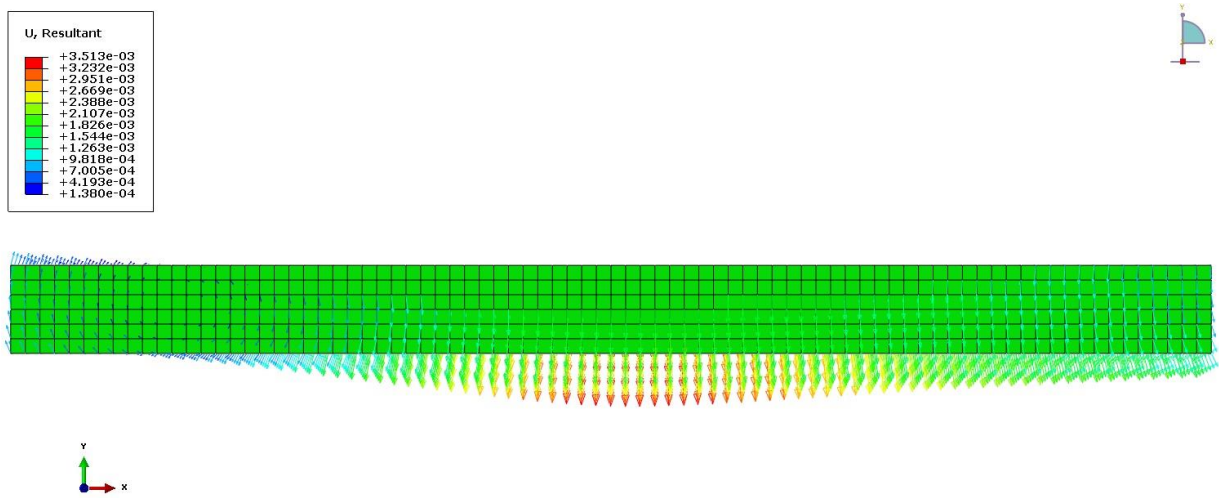
**Figure 9** Deflection of critical sleeper (47) in relation to location of load

598

599

600

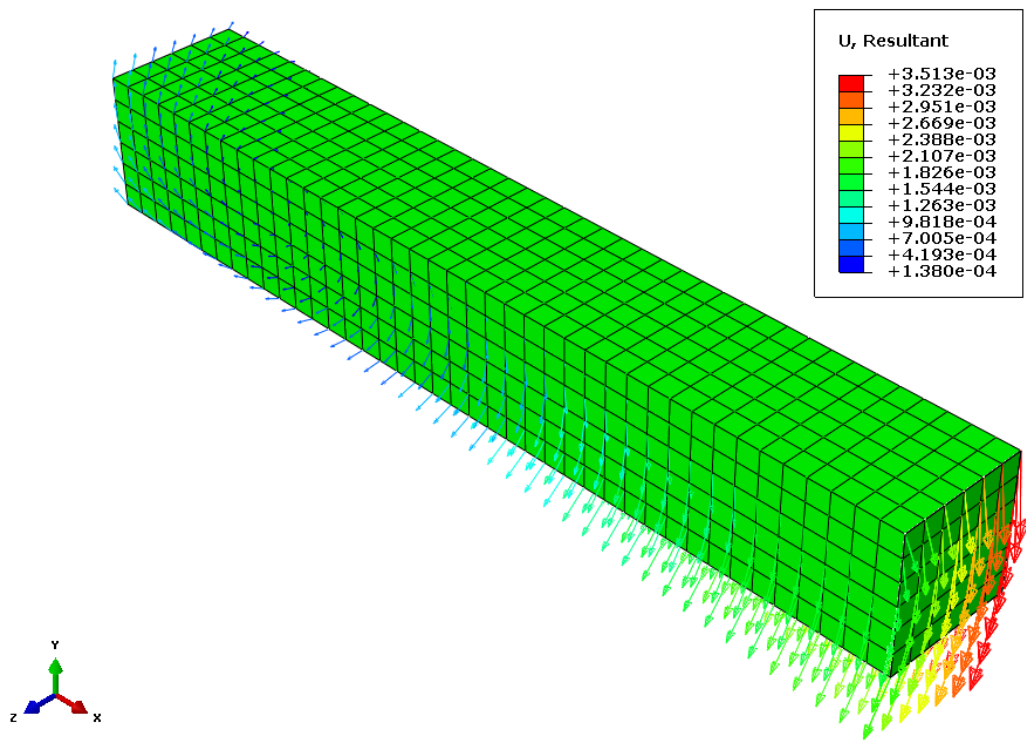
601



602

**Figure 10** Deflection mode of critical sleeper - XY plane

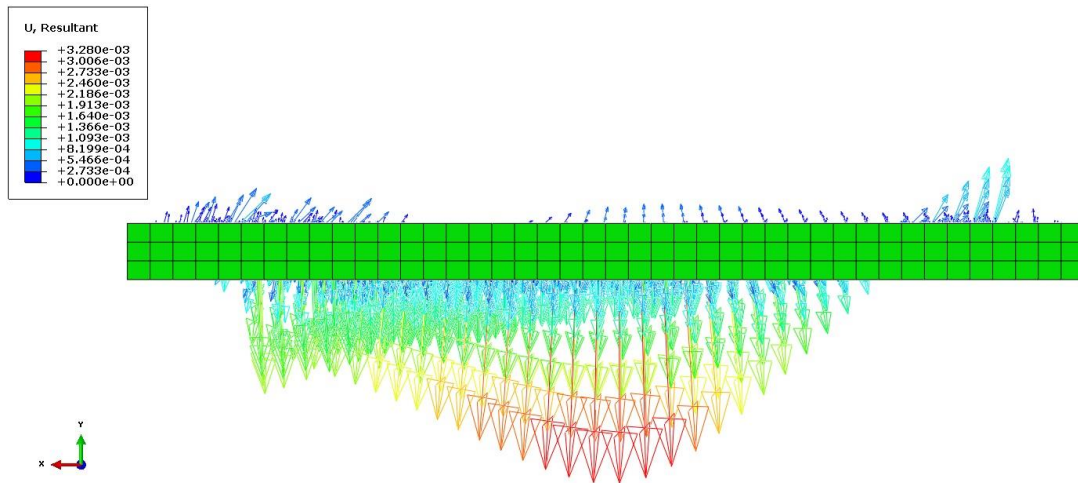
603



604

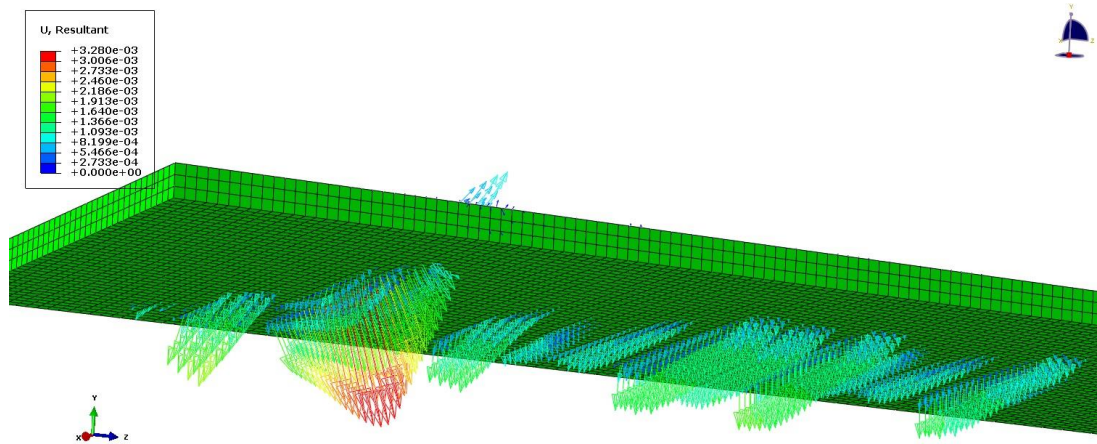
**Figure 11** Deflection mode of critical sleeper – 3D plane centre cut view

605  
606  
607  
608  
609  
610  
611  
612  
613  
614  
615  
616  
617  
618  
619  
620  
621  
622  
623  
624  
625  
626  
627



a) Deflection of ballast layer for critical loading - XY plane

628



b) Deflection of ballast layer for critical loading - 3D plane

629

630

631

632

633

634

635

636

637

638

639

640

641

642

643

644

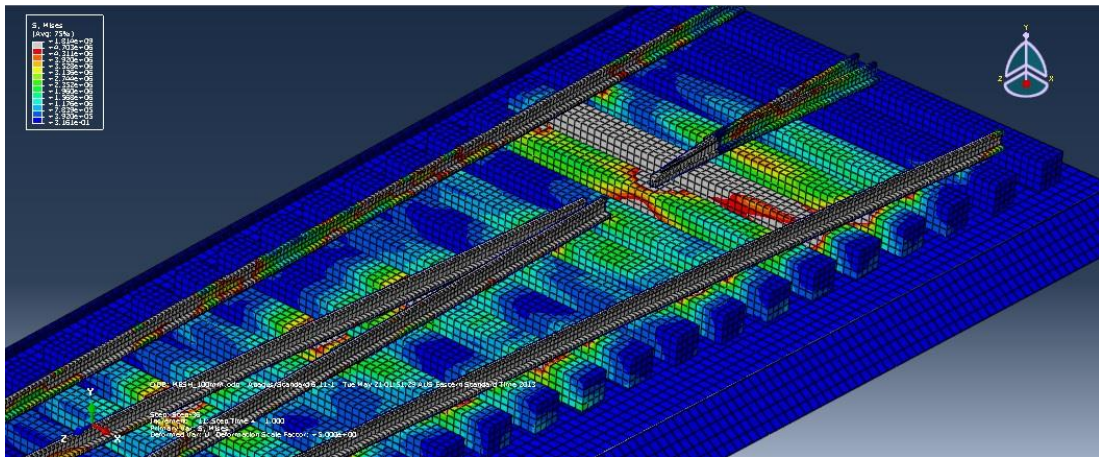
645

646

**Figure 12** Deflections of ballast layer



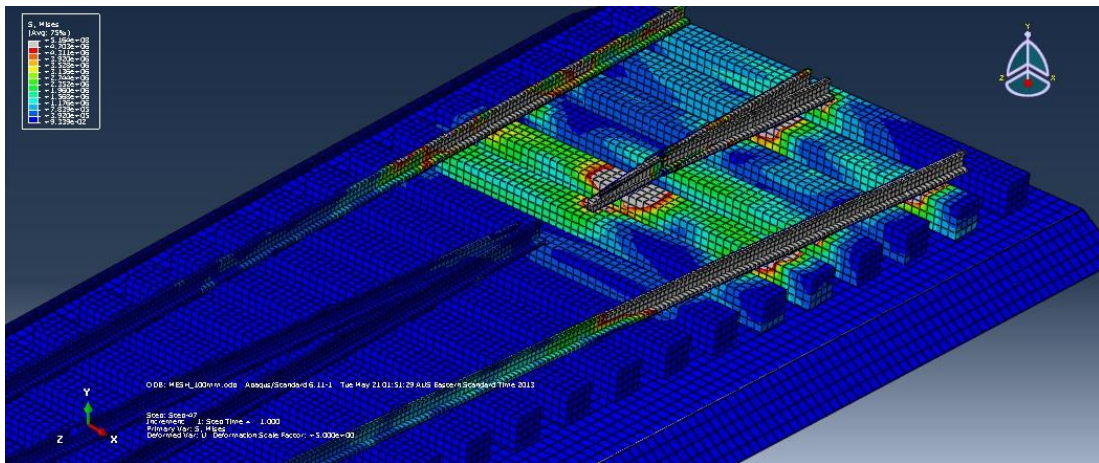
647



648

a) Stress distribution at load step 36 for 100mm meshed ballast (when the wheel runs over the crossing nose)

649



650

b) Stress distribution at load step 47 for 100mm meshed ballast (when the wheel runs further away from the crossing nose)

651

652

653

654

655

656

**Figure 13** Shear stresses of turnout sleepers